C. R. Physique 18 (2017) 86–97

Contents lists available at ScienceDirect

Comptes Rendus Physique

www.sciencedirect.com

Energy and radiosciences / Énergie et radiosciences

On energy harvesting for augmented tags

Récupération d'énergie pour tags augmentés

Dahmane Allane [a,b,*], Yvan Duroc [c], Gianfranco Andia Vera [b], Rachida Touhami [a], Smail Tedjini [b]

[a] *Université des sciences et de la technologie Houari-Boumédiène (USTHB), Algeria*
[b] *Laboratoire de conception et d'intégration des systèmes (LCIS), part Grenoble Institute of Technology of University Grenoble-Alpes, Valence, France*
[c] *Ampere Lab, Lyon University, Villeurbanne, France*

ARTICLE INFO

Article history:
Available online 23 December 2016

Keywords:
Energy harvesting
RFID UHF
Non-linearity
Harmonics
Sensor-tags

Mots-clés :
Récupération d'énergie
RFID UHF
Non-linearités
Harmoniques
Tags-capteurs

ABSTRACT

In this paper, the harmonic signals generated by UHF RFID chips, usually considered as spurious effects and unused, are exploited. Indeed, the harmonic signals are harvested to feed a supplementary circuitry associated with a passive RFID tag. Two approaches are presented and compared. In the first one, the third-harmonic signal is combined with an external 2.45-GHz Wi-Fi signal. The integration is done in such a way that the composite signal boosts the conversion efficiency of the energy harvester. In the second approach, the third-harmonic signal is used as the only source of a harvester that energizes a commercial temperature sensor associated with the tag. The design procedures of the two "augmented-tag" approaches are presented. The performance of each system is simulated with ADS software, and using Harmonic Balance tool (HB), the results obtained in simulation and measurements are compared also.

RÉSUMÉ

Dans cet article, les signaux harmoniques générés par les puces RFID UHF, généralement considérés comme des effets parasites et non utilisés, sont exploités. En effet, les signaux harmoniques sont collectés pour alimenter un circuit supplémentaire associé à un tag RFID passif. Deux approches sont présentées et comparées. Dans la première approche, le signal harmonique $3f_0$ est combiné avec un signal Wi-Fi externe à 2,45 GHz. L'intégration se fait de telle manière que le signal composite augmente le rendement de conversion du circuit de récupération d'énergie. Dans la seconde approche, le signal harmonique $3f_0$ est utilisé comme seule source d'énergie alimentant un capteur de température commercial associé au tag. Les procédures de conception des deux « tags augmentés » sont présentées. Les performances de chaque système sont simulées avec le logiciel ADS, en utilisant l'outil

* Corresponding author at: Université des sciences et de la technologie Houari-Boumédiène (USTHB), Algeria.
E-mail address: allane.dahmane@hotmail.fr (D. Allane).

http://dx.doi.org/10.1016/j.crhy.2016.11.007
1631-0705/

Harmonique Balance (HB) ; les résultats obtenus au moyen de simulations et de mesures sont aussi comparés.

1. Introduction

With the emergence of the Internet of Things and its 50 billion connected objects expected for 2020, the RFID (Radio Frequency Identification) technology, well known in the areas of traceability, logistics and security, presents promising enabling perspectives [1,2]. Indeed, UHF (Ultra High Frequency) RFID, with its huge and relevant features (standardized, mature wireless and passive technology), is rapidly evolving to new types of tags, the so-called "augmented tags", which provide more than ID by incorporating not only the unitary identification function, but also new capabilities such as localization and sensing. The idea of the sensor-tag approach is to associate new tag information capture capabilities while still enjoying the identification functionality and obviously, also the remote power supply and wireless transmission. A wide variety of RFID Sensors have been demonstrated in the literature, among them sensors for temperature [3,4], pressure [5], humidity [6,7], deformation [8], crack width [9], curvature monitoring [10], Open/Close [11], chemical [12], food quality [13], etc. The previous references give some examples of the cited functionalities, but the list is not exhaustive.

To transform a passive RFID tag into a passive RFID sensor tag, there are two types of implementations. In the first type, one can exploit the sensitivity of the tag antenna to its environment, in particular when the antenna is made or loaded by sensitive material [14] or to profit from the nonlinear RFID chip properties. In the second type, the tag integrates an external sensor, which requires some additional energy consumption [15–20]. In this second case, when using the chip rectifier, the difficulties reside on the energy supply of the attached sensor to the detriment of tag performance. Another alternative is the use of energy-recovery devices that leverage energy from other sources such as solar, thermal, kinetic or electromagnetic sources [21,22]. Besides, the integration of the sensor in the RFID chip is also an interesting alternative, even if it leads to a reduction in the read range due to the degradation of the backscattering signal. This is why some recent studies focus on the co-optimization of communication and sensing characteristics. These new approaches aim to divide and/or modify the encoding of the information returned by the tag in order to combine the advantages of each; for instance, using a phase modulation for the sensor functionality and an amplitude modulation for the communication [9] or carrying the sensor information through a modulation frequency [23]. Another approach is a hybrid analog–digital backscatter platform that uses digital backscatter for addressability and control, but switches to analog backscatter mode for high data rate transmission sensor data [24]. It is also worth citing the widely used Wireless Identification and Sensing Platform (WISP), which is a programmable, microcontroller-based sensor tag compliant with the EPC Class 1 Generation 2 UHF RFID standard [25]. Furthermore, tags with battery-assisted passive (BAP) mode are now available and enable longer read-range sensing and several commercial BAP Gen2 integrated circuits have a serial port [19].

This paper focuses on the case where the RFID tag integrates one or several specific sensors. In this context, offering new sensing capabilities in RFID is synonym of additional energy needs in order to preserve the performance, and especially, the hallmark of passive tags. Some works demonstrated that it is possible to exploit green energy sources such as solar, thermal or mechanical sources. Electromagnetic energy (EM) sources present either in the environment of tags or within them (so unexploited and classically lost) are here used, and in this sense the proposed solutions could be considered green too. Indeed, the harmonic signals generated by the UHF RFID chips, and especially, the third-harmonic signal, which is the dominant harmonic [26,27], becomes useful in order to (*i*) significantly improve the EM harvesting operation via an external source or (*ii*) directly provide energy source for a sensor associated with the tag.

This work, which strongly mixes energy and radio science (i.e. power supply and wireless sensors-tags) in terms of new proposed concepts and technological solutions, constitutes a relevant brick for this dossier devoted by URSI France to "Energy and Radio Science". The paper is organized as follows. In section 2, some considerations on the use of nonlinear circuits and associated applications are summarized with a focus on the RFID context in order to better highlight the proposed concept. Section 3 presents the two envisaged system configurations exploiting the nonlinear behavior of UHF RFID chips. Section 4 explains the fundamental steps of the design and highlights the methodology. The modeling of the UHF RFID chip taking into account the impedances at operating frequencies and the harmonics generation is detailed. The two harvesting circuits, which are distinct according to the application, are described, justifying the choice and highlighting the main characteristics. The coupling with a three-port matching network between reader, chip and harvesting section, which is a critical design step, is detailed, comparing notably the performance of lumped and distributed solutions. Section 5 demonstrates the proposed concepts and shows the performance results in simulation and measurement. Finally, section 6 draws the conclusion and perspectives.

2. Considerations on the use of nonlinearities in radar, sensing and RFID applications

The signal generation by nonlinear behavior (i.e. harmonics or/and intermodulation products) is a well-known phenomenon that has been extensively studied in active antennas and circuit literature. Harmonic radar (also called secondary

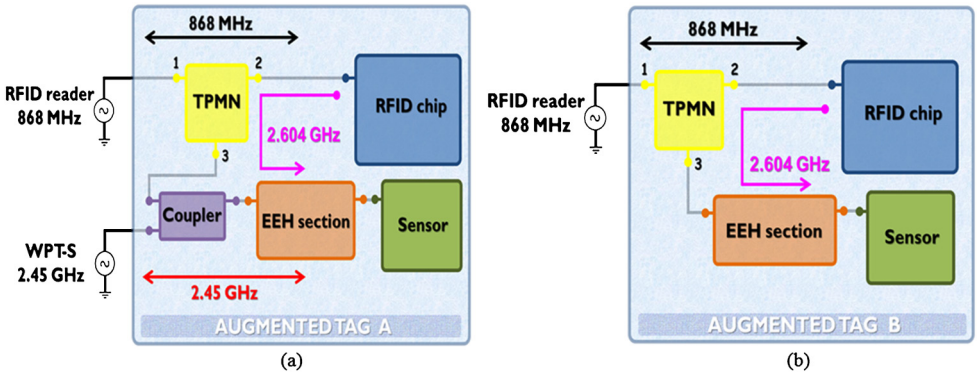

Fig. 1. Proposed augmented tags: (a) multi-sources harvesting system (augmented tag A); (b) third-harmonic harvesting system (augmented tag B).

radar), first presented in 1967 [28], constitutes an emblematic application of the use of backscattered modulation exploiting the nonlinearity. The principle is that the radar illuminates the target at a fundamental tone, and measures the reflection at one or several harmonic frequencies. Transponders incorporating nonlinear components are used, e.g., for rectification, harmonic transponders, and intermodulation sensors. Several recent works by Vikarii describe the use of intermodulation for the optimization of wireless sensors and the characterization of transponder antennas, but also the design of harmonic tags [29–31], showing the great potential of this approach and also remembering the main works on the topic. It is worth noting that harmonic radar can allow the detection of objects that inherently produce a harmonic response (such as steel reinforcement in concrete structures [32]), or also can be used with specific transponders designed to produce a strong harmonic response. In RFID context, one notices that the nonlinear property of the integrated circuit front-end due to the Schottky diode-based rectifier structure (i.e. the voltage multiplier) can be exploited in a contactless radiation pattern technique [33]. Harmonic generation was also used in frequency-doubler tags, also known as one-bit RFID tags, applied to check and monitor the possible presence of a tag in the interrogation zone of a reader, [34,35]. Another possible application is the use of intermodulation distortion for location by triangulation of a tag from three readers [36].

The first experimental characterization of the nonlinearities produced by passive UHF RFID tags was presented by Nikitin et al. in 2009 [37]. The objective of this work was to quantify the level of harmonic backscattering from passive tags, used for tagging airplane parts and cabin items, susceptible to interfere with aircraft systems and components. Indeed, RFID transponders rectify dc voltage from the received RF signal to operate their digital circuits, and the rectifier is also used as a modulator in the modulated backscattering principle of RFID. Consequently, a typical passive RFID tag consists of an antenna directly connected to an integrated circuit with nonlinear RF front-end. A tag can backscatter harmonics and intermodulation products when interrogated with the modulated and unmodulated reader signal. In order to postulate and demonstrate the possible exploitation of harmonic signals produced by passive UHF RFID tags, the authors completed the characterization methodology proposed by Nikitin et al. and quantified the harmonic levels considering new measurement protocols in radiated and conducted cases [26,27]. Given the non-negligible and even potentially exploitable power level of the third-harmonic signal, additional works have been proposed with the aim both to present a complete theoretical analysis of the harmonics generation in UHF RFID chips and also to introduce several possible applications in the field of communication channel diversity, authentication, localization or sensing [38–40]. In this paper, two strategies of managing the third-harmonic signal energy dedicated to augmented UHF RFID tags are presented, with an experimental demonstration.

3. Strategies to manage the third-harmonic signal energy

3.1. Multi-source harvesting approach

For the first presented system, the sensor is supposed to be mainly energized by an ambient RF source. The well-known idea is to take advantage of the ever-increasing amount of EM radiation present in our environment due to the ubiquitous wireless communication devices. Among the most frequently encountered frequency bands situated around 900/1800 MHz, 2 GHz and 2.45 GHz (corresponding to standards GSM/DCS, UMTS, and WLAN respectively), the 2.45 GHz frequency is particularly chosen because of its proximity to the third-harmonic frequency of UHF RFID. Indeed, mixing these two sources could significantly improve the RF-to-dc conversion efficiency, as it has demonstrated in previous works [41,42].

The augmented tag, illustrated in Fig. 1a and the so-called augmented tag A in the hereinafter, is comprised of two main parts: (i) an RFID section conventionally composed by a passive UHF RFID chip interrogated by an RFID reader operating at 868 MHz (corresponding to the European standard); (ii) an EM Energy Harvesting (EEH) section comprised of a microwave rectifier centered at the frequency of a Wireless Power Transmitter Source (WPT-S), i.e. 2.45 GHz. Note that the rectifier stage of the RFID chip is modeled by a diode-based voltage doubler with four stages for simulation studies, while a commercial chip is used to validate experimentally the model. Both sections are connected through a Three-Port Matching Network

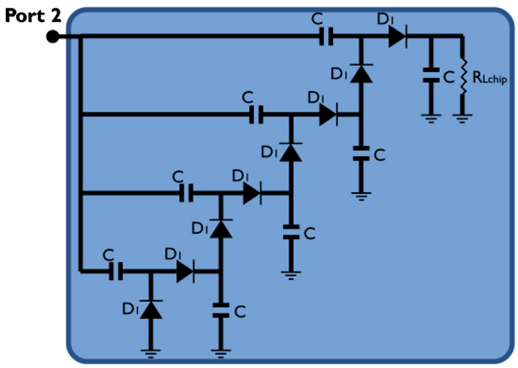

Fig. 2. The RFID chip model using four Schottky doubler stages.

Table 1
Comparison between the input impedance of the real chip and the chip model at f_0 and $3f_0$.

	f_0	$3f_0$
Z_{in} (measure)	$15 - j115$	$7 - j2$
Z_{in} (model)	$13 - j95$	$3 - j2$

(TPMN), which allows: the impedance matching of the chip to the antenna at 868 MHz; and to the 50 Ω coupler impedance at 2.604 GHz. Hereinafter the third harmonic of 868 MHz, i.e. 2604 MHz, is denoted by $3f_0$. The directional coupler is used in order to combine $3f_0$ with the 2.45-GHz signal at the input of the rectifier in order to optimize conversion efficiency [41,42]. It is worth noting that the design of the matching network relies on an accurate characterization of each element to be interconnected and represents one of main challenges for the realization.

The overall system is designed to maximize the RF-to-dc power conversion efficiency of the energy harvesting circuit (EEH-a) denoted by η_a, defined as the ratio of the dc output power to the RF power available at the input of EEH-a.

3.2. Harmonic harvesting approach

Contrary to conventional solutions that consist in the addition of an external power source (e.g., battery or energy harvesting system), the second approach, hereinafter so-called augmented tag B, only exploits the power carried by $3f_0$ [43]. Its configuration, shown in Fig. 1b is similar to that in Fig. 1a, except that the EEH section has only one input, i.e. the $3f_0$ generated by the chip. The chip model is the same as the one used in the previous approach.

The TPMN, a key stage of the system integration, enables a dual impedance matching of the RFID chip: at 868 MHz with the tag antenna impedance, and also, at $3f_0$ with the microwave rectifier.

The EEH-b rectifier is optimized at $3f_0$. A single-diode structure is used in order to maximize power conversion efficiency, given that the $3f_0$ level is relatively low.

For the sake of clarity, the sub-components of the augmented tags A and B will be identified by the letters A and B, respectively.

4. Design methodology

Advanced Design Software (ADS) simulation tools from Keysight are used for the design of each section.

4.1. RFID chip model

In order to reproduce the input impedance of the real chip (EM4325 from EM Microelectronic) [44], at f_0 and $3f_0$, and also to reproduce its non-linear behavior (i.e. the harmonic signals production), the real chip is modeled using a four-doubler-stage rectifier circuit with a configuration similar to the one used in the Dickson charge pump (see Fig. 2).

As detailed in [40], and [43], from the measured values of the input impedance and using the Large-Signal S-Parameters (LSSP) and Harmonic Balance (HB) tools, the RFID chip model is optimized at 868 MHz and for an −9 dBm input power in the first configuration and for 0 dBm in the second configuration. In [43], a comparison between the real and the imaginary parts of the input impedance of the real chip and the ones of the designed model over a wide frequency range is performed, in the case where the input power source is 0 dBm. Table 1 shows the values of the input impedance obtained at f_0 and $3f_0$ for the real chip and the chip model. As we can remark, the obtained values are quite similar and have the same order of magnitude. So, the simplified model will be used for the simulation hereinafter.

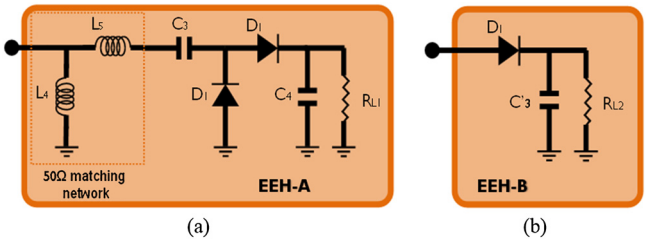

Fig. 3. EEH section of (a) augmented tag A and (b) augmented tag B.

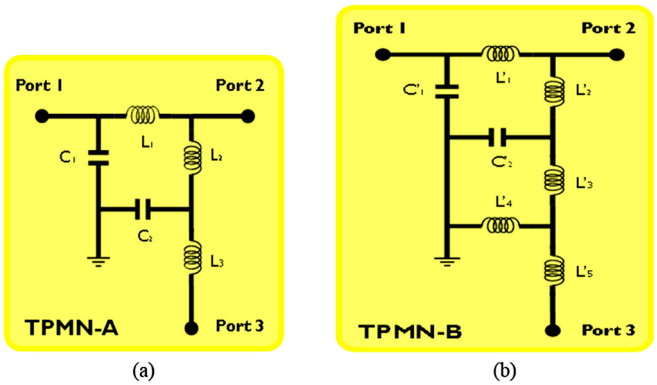

Fig. 4. TPMN circuit topology used for (a) augmented tag A and (b) augmented tag B.

4.2. Design of the electromagnetic energy harvesting section

The architecture of the rectifier and the choice of the diode are essential here. Microwave rectifiers have different topologies, depending on the position and number of the HF diodes. The simplest and most common configurations are series or shunt-mounted single diodes because they present good performance for very low incident power. For higher power levels, a doubler-stage even bridge-type rectifier offers better performances. Moreover, the diode is the main source of loss and its characteristics will determine the overall performance of the rectifier. RF-to-dc power conversion efficiency is mainly determined by: the series resistance (R_s), which limits the efficiency; the zero-bias junction capacitance (C_{j0}), which affects the way the harmonic currents oscillate through the diode; and breakdown voltage (V_B) which limits the power handling capability of the rectifier circuit. A rectifying diode has to also present high speed switching characteristics in order to follow the frequency of input signal and have a low threshold voltage (V_F) to operate at a low RF input power.

Considering these specifications and requirements, firstly a SMS7630 Schottky diode from Skyworks was selected: $R_S = 20\ \Omega$; $C_{j0} = 0.14$ pF; $V_B = 1$ V; $V_F = 60$ mV. Then the EEH sections were designed as follows. The EEH section of the augmented tag A, which is mainly designed to harvest the signal from the source at 2.45 GHz (at which the $3f_0$ harmonic signal is combined), is comprised of a microwave rectifier centered at 2.45 GHz (EEH-A, Fig. 3a), matched to 50 Ω through L4 and L5 inductors, and based on one doubler stage. On the other hand, the EEH section of the augmented tag B is designed to harvest only the $3f_0$ harmonic signal reflected from the RFID chip. It is composed of a microwave rectifier centered at 2.604 GHz (EEH-B, Fig. 3b), and based on a Schottky diode in order to maximize its power conversion efficiency. RL2 value (3.3 kΩ) represents the input resistance of two blocks connected in series, a power management module, and a commercial temperature sensor.

4.3. Design of the three-port matching network

One of the key challenges for the two proposed systems is the TPMN design. For the two configurations illustrated in Fig. 1, the TPMN has to realize three functions: (*i*) impedance matching between ports 1 and 2 at $f_0 = 868$ MHz, (*ii*) impedance matching between ports 2 and 3 at $3f_0 = 2.604$ GHz, and (*iii*) isolation between ports 1 and 3 at f_0.

Fig. 4a and Fig. 4b illustrate the two TPMN-A and TPMN-B topologies used for the augmented tags A and B, respectively. The first circuit (Fig. 4a) is mainly designed both to match ports 1 and 2 at f_0 through the filter (L1, C1), and to match ports 2 and 3 at $3f_0$ thanks to the filter (L2, C2, L3). This circuit is simpler than the one for the second configuration, but it presents a poor isolation between ports 1 and 3 at f_0. However, its performance is sufficient in order to ensure that the chip remains active. For the second configuration (augmented tag B), a better isolation between the ports 1 and 3 is absolutely required in order to evaluate the contribution of the third harmonic. This is why the first circuit is completed with the two inductors L'4 and L'5 (Fig. 4b).

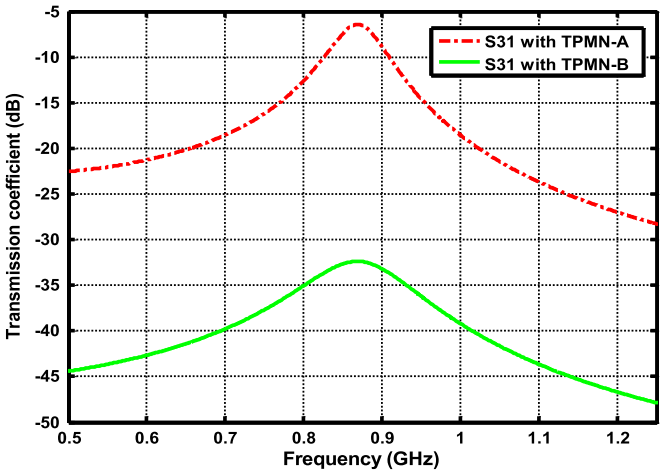

Fig. 5. Comparison of the simulated transmission coefficients S31 obtained with TPMN-A and TPMN-B.

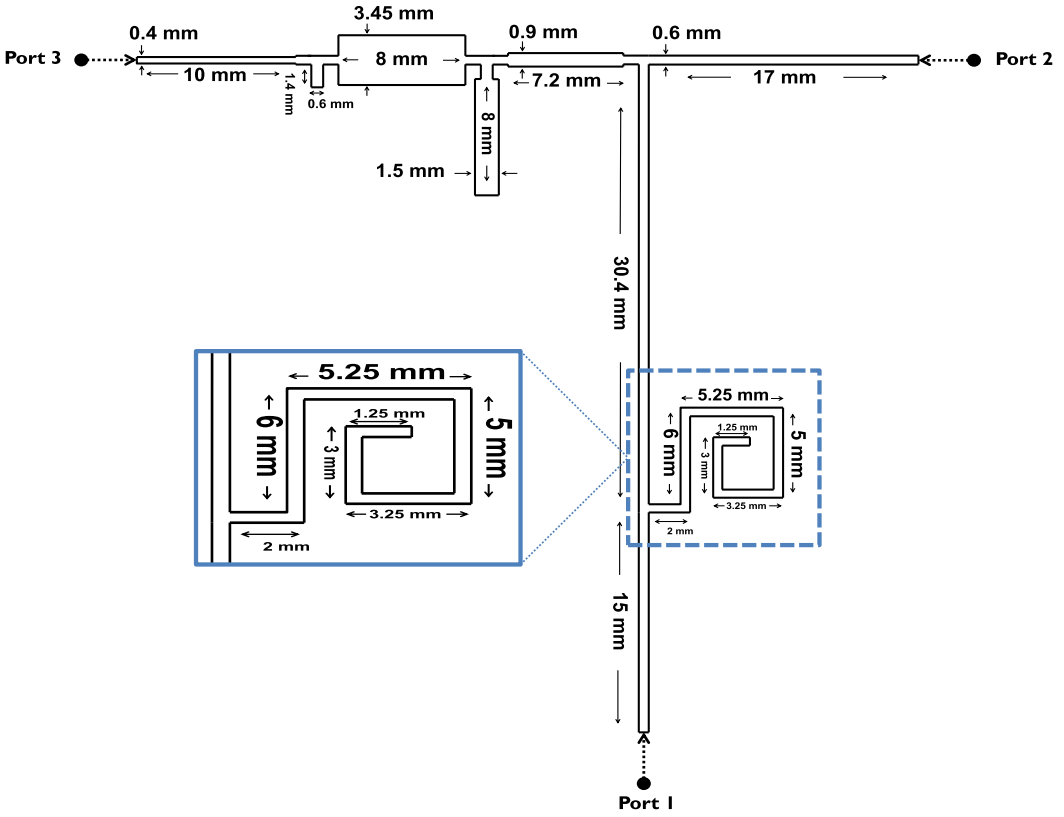

Fig. 6. Transmission line section dimensions of the equivalent distributed TPMN-B circuit.

The two TPMN circuits show similar performance for S21 and S32 coefficients. The difference only concerns the S31 coefficient and so the isolation between ports 1 and 3 that is measured as $-$S31 (dB). At f_0, the isolation is 7 dB using topology (a) and 33 dB using topology (b), as shown in Fig. 5.

The prototype of the augmented tag B is finally realized using a TPMN-B designed with the distributed elements (Fig. 6). Indeed, transmission line sections exhibit a high-quality factor compared to commercially available lumped components, and consequently limit the TPMN-B transmission losses. In practice, the Duroid 5880 substrate with a thickness of 0.8 mm, a dielectric permittivity of 2.2, and a low loss factor of 0.0009 is used.

Fig. 7 presents a comparison between the lumped and distributed TPMN-B circuits in terms of the simulated reflection coefficients S11, S22, S33 and the simulated transmission coefficients S21, S32, S31.

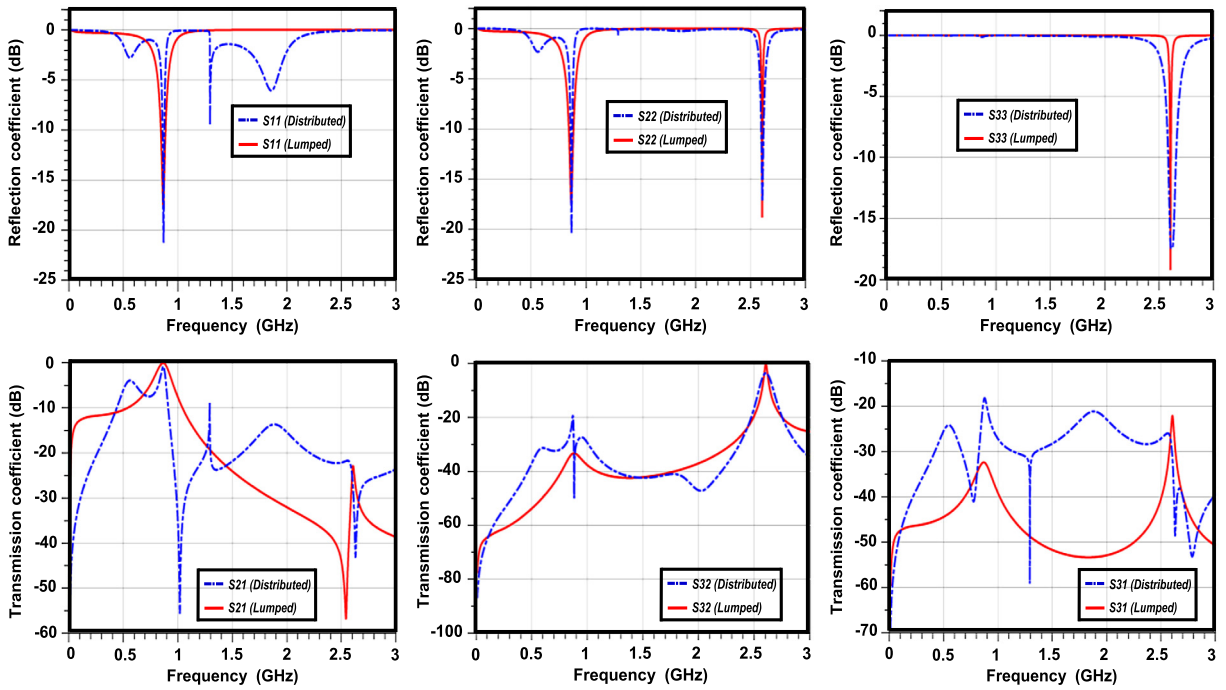

Fig. 7. Comparison between the simulated reflection coefficients S11, S22, S33 and the transmission coefficients S21, S32, S31 obtained with lumped TPMN-B and the distributed equivalent circuit.

Table 2
Comparison between transmission and reflection coefficients obtained with lumped TPMN-B and distributed equivalent TPMN-B at f_0 and $3f_0$.

	At f_0		At $3f_0$	
	Lumped TPMN-B	Distributed TPMN-B	Lumped TPMN-B	Distributed TPMN-B
S11 (dB)	−17.2	−21.2	0	0
S22 (dB)	−17.2	−20.4	−18.5	−16.4
S33 (dB)	0	0	−19	−17
S21 (dB)	0	−0.8	−23	−26.7
S32 (dB)	−33.4	−18.8	0	−2.2
S31 (dB)	−32.4	−19	−22	−31.2

Table 2 summarizes the coefficient values obtained with the two TPMN-B structures at f_0 and $3f_0$. The results show a good agreement, and therefore validate the design of the equivalent distributed TPMN-B circuit.

5. Performance evaluation

5.1. Multi-sources harvesting system – augmented tag A

The aim of this section is to evaluate the power conversion efficiency, denoted by η_a, of microwave rectifier EEH-A for the proposed augmented tag A configuration (Fig. 1a).

The first step is to interconnect all the designed sections together and to perform an HB analysis in order to check the Power Spectral Density (PSD) at the entrance to the EEH-A microwave rectifier.

For this analysis two reader power levels are used:

- −9 dBm (Reader min), which corresponds to the activation power of the used chip (EM4325),
- 5 dBm (Reader max) which is the power received at 1 m from a reader that emits the maximum allowed power (31.5 dBm) by the European Telecommunications Standards Institute (ETSI).

Fig. 8 illustrates the odd harmonics levels at the EEH-A section input as a function of the frequency. Three main signals are observed: the signal at $3f_0$, which is redirected thanks to the TPMN circuit; the signal at 2.45 GHz from the external source; and the signal at f_0 from the RFID reader, which coupled when the reader transmits the allowed maximum power.

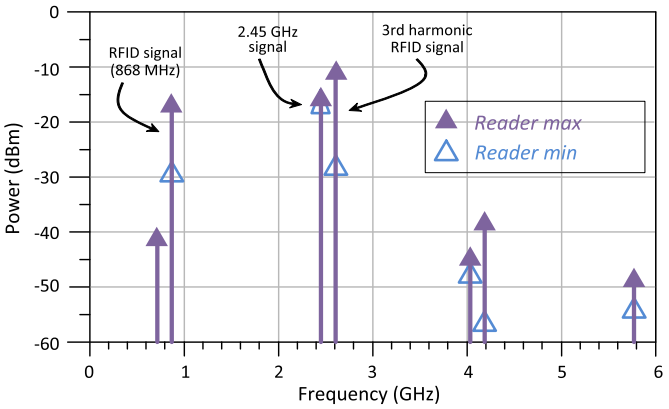

Fig. 8. Odd harmonics levels at the EEH-A section input as function of frequency.

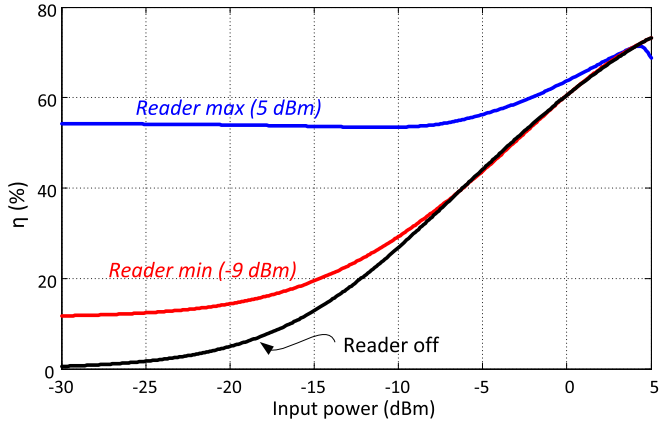

Fig. 9. Power conversion efficiency η_a of the EEH-A section simulated with a chip model as a function of the WPT-S power.

The remaining signals are high-order harmonics and intermodulation products, which have low power amplitudes and are considered here as negligible for the calculation of η_a, as presented below. The levels of the even harmonics are less than -45 dBm, and therefore are not considered [40].

The power conversion efficiency η_a of the EEH-A circuit is deduced from the PSD, considering the dominant RF signals power at its input, and defined as follows:

$$\eta_a = \frac{P_{dc}}{P_{RF}} = \frac{P_{dc}}{P_{RF@0.868} + P_{RF@2.45} + P_{RF@2.604}} \tag{1}$$

where $P_{RF@0.868}$ is the power leaked from the reader, $P_{RF@2.45}$ is the power coming from the WPT-S source, and $P_{RF@2.604}$ is the $3f_0$ chip harmonic signal power.

Using (1), η_a at 2.45 GHz was simulated as a function of the input power source for three different configurations (Fig. 9):

- Case 1: the source at 2.45 GHz is the single power source;
- Case 2: the source at 2.45 GHz is combined with a reader that emits -9 dBm (Reader min);
- Case 3: the source at 2.45 GHz is combined with a reader that emits 5 dBm (Reader max).

When the source at 2.45 GHz is providing -30 dBm, the simulation results show that η_a increases from 1% when the RFID reader is turned off to 17% when the reader transmits -9 dBm, to 56% when the reader transmits 5 dBm. The more the reader emits power, the more efficiency is improved. This is explained by the fact that when the reader power becomes greater, the $3f_0$ signal power reflected from the RFID chip becomes greater also. The signal at $3f_0$ is redirected into the EEH-A circuit, which improves power conversion efficiency.

For the experimental part, an emulation of the system has been achieved [40]. The emulated prototype is built as follows. For the RFID section, a RFID reader source at 868 MHz and a real commercial chip (EM4325) are used. The tag antenna is emulated by two impedance tuners for the matching between reader, chip and EEH section. For the harvesting section, the Wi-Fi source signal at 2.45 GHz is emulated by a source generator and a 50 Ω coupler combines the two signals at the entrance to the EEH section (i.e. the 2.45 GHz signal and the third-harmonic one reflected from the EM4325 chip and

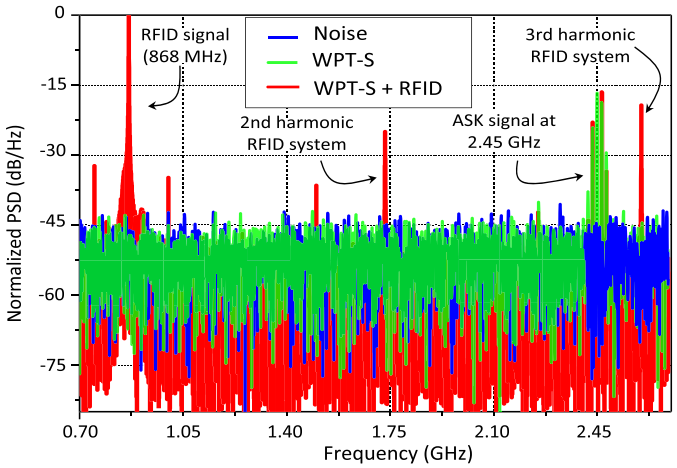

Fig. 10. Normalized power spectral density (PSD) at the EEH-A section input as a function of the frequency [40].

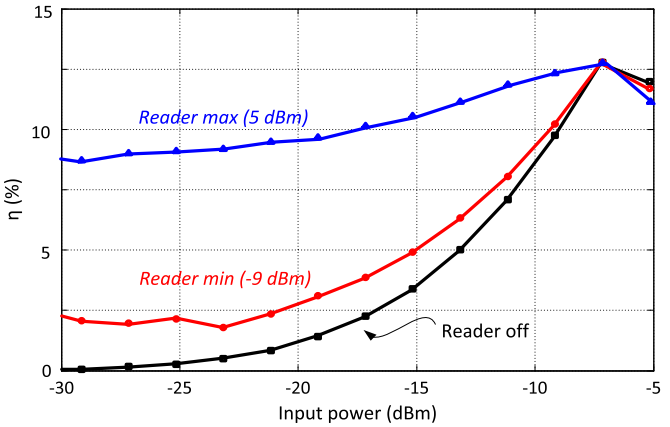

Fig. 11. Power conversion efficiency η_a of the EEH-A section measured with a real commercial chip as a function of the WPT-S power.

redirected into the coupler by the TPMN-A). The EEH section (i.e. a single stage doubler microwave rectifier centered at 2.45 GHz) is designed on Arlon A25N substrate.

Fig. 10 illustrates the normalized PSD obtained at the EEH-A section input. As previously, using (1), η_a is deduced and illustrated in Fig. 11 as a function of the input power source at 2.45 GHz. The experimental results also show a better efficiency in cooperative operation with 8% improvement in η_a when the reader switches from off-operation to a power source transmitting 5 dBm, under −30 dBm at 2.45 GHz. It is worth noting that the magnitudes of the efficiency achieved by measurements for the three considered cases are lower than the ones obtained by simulation. This is due to the fact that the system has not been realized, but emulated. On the other hand, it can be noticed that the curves reproduce exactly the same trend as in the simulation, namely, when the reader emits more power, η_a is improving.

The proposed concept consisting to exploit the third-harmonic signal combined with the WPT-S in order to improve the rectifier efficiency dedicated to the feed of a sensor associated with a RFID UHF tag is consequently validated. The improvement is particularly significant for lower power levels of the WPT-S source.

Finally, the presented results highlight the interest to combine the harmonic signal $3f_0$ (classically not used, i.e. unexploited and even lost) with an external power source at 2.45 GHz making a waveform more chaotic with a higher PAPR (peak-to-average power ratio).

5.2. Harmonic harvesting system – augmented tag B

1) *System performance evaluation*

The aim of this section is to evaluate the dc performance of the EEH-B microwave rectifier dedicated to the third-harmonic rectification in the proposed augmented tag B configuration (Fig. 1b).

The first step in the validation of the proposed design is the evaluation of the harmonic signals distribution at port 2 (i.e. the RFID chip input) and port 3 (i.e. the EEH-B section input) of the system. As for the first configuration, all the designed

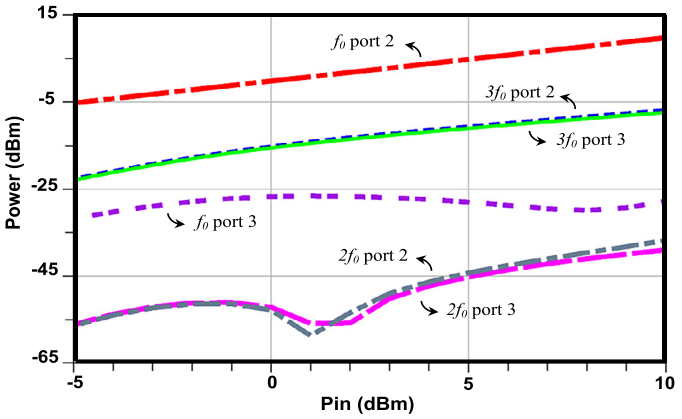

Fig. 12. Simulated PSD at ports 2 and 3 of the system as a function of the input power at f_0.

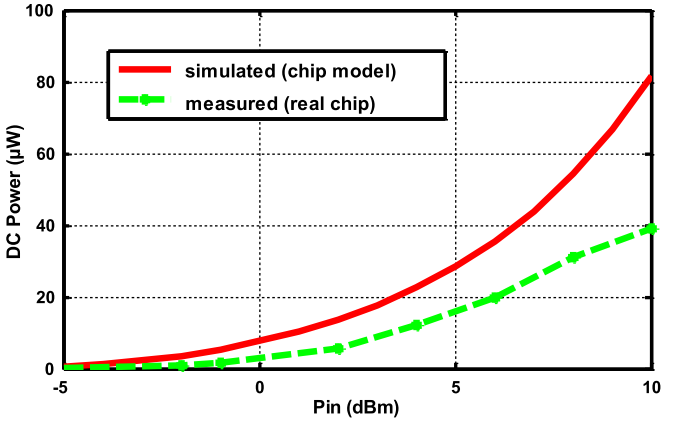

Fig. 13. Dc harvested power from the third-harmonic signal rectification as a function of the input power source.

sections are interconnected and an HB analysis is performed. For an input power at 868 MHz from −20 dBm to 10 dBm, Fig. 12 illustrates the PSD for the ports 2 and 3. The harmonic signal at $3f_0$ reflected at port 2 is completely redirected to port 3 whatever the input power source level, and also the signal at f_0 coupled at the port 3 is very low. The TPMN-B section provides a very good isolation of port 3 from the fundamental f_0 signal.

In order to evaluate the dc performance of the EEH-B section, Fig. 13 shows the dc harvested power at its output versus the input power applied to the tag at f_0; it is worth noting that for input power levels less than −5 dBm, there is no harvested dc-power [43]. Differences are observed between simulation results (using the presented chip model) and measurement (using a real RFID chip), because if the chip model reproduces similar impedances at f_0 and $3f_0$, it does not exactly reproduce the same non-linear behavior with a different power level generated at $3f_0$. Based on the proposed concept, experimental tests show an achieved dc power of 39 µW when the reader transmits 10 dBm at f_0 from the sole contribution of the third harmonic.

2) *Application case*

In order to conclude the study and highlight the proposed concept, the goal is now to use the dc power recovered from the only $3f_0$ harmonic signal to power up a commercial temperature sensor. As often in practical applications, the microwave rectifier (EEH-B) is not able to provide enough energy continuously to the sensor. Consequently, a power management module, that can store energy and deliver it to the sensor at regular times, is used, but itself is powered up without additional energy source.

Fig. 14 presents the overall configuration where a RFID reader emits power exploited by the augmented tag B that is associated with a PSG03551 temperature sensor and a BQ25504EVM-674 power management module. The experimentation shows that, with an emitted power of 35 dBm, the temperature sensor is operational up to a distance of 80 cm, while consuming 60 µW in measuring mode every 10 s.

6. Conclusion

In the context of the rapid development of the so-called augmented tags, i.e. tags that integrate more than ID capabilities in particular sensing, the paper demonstrates how the harmonic signals generated by the UHF RFID chip could be benefi-

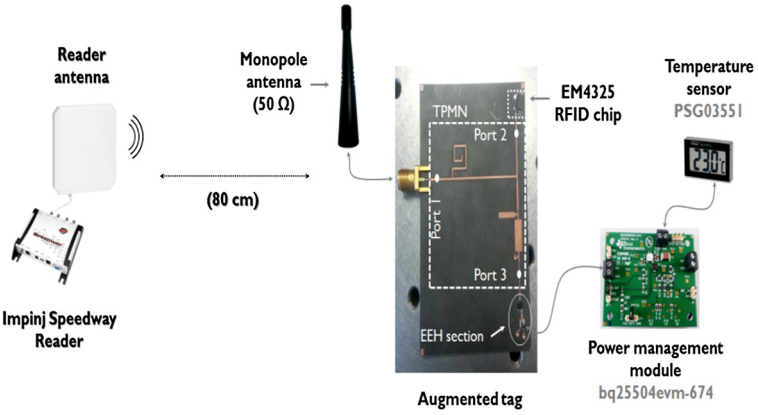

Fig. 14. Evaluation setup of the augmented tag B supplying a commercial temperature sensor.

cially exploited. Several strategies can be considered for such exploitation. More specifically, two concepts are evaluated in this paper.

The first concept aims to combine two signals close in frequency in order to get a more chaotic signal at the input of the rectifier dedicated to the sensor, and consequently to improve the RF-to-dc conversion efficiency. In practice, the main signal is from an external source at the ISM frequency of 2.45 GHz (such as ubiquitous WLAN source), and the second signal at $3f_0$ (i.e. 3×868 MHz $= 2604$ MHz) is generated by the nonlinear behavior of the RFID chip. In this case, a significant improvement of the conversion efficiency is observed.

The second demonstrated concept exploits only the $3f_0$ harmonic signal produced by the UHF RFID chip in order to supply a commercial temperature sensor associated with a tag. The operation is shown possible thanks to the use of a power management module. So, we demonstrate that the generated third harmonic can be used as source of energy for an external sensor.

The presented studies exploiting the third-harmonic signal energy in passive UHF RFID tags open new ways for optimizing potential EM energy sources in near or far-field environments. The proposed concept of the exploitation of the harmonic signals generated by the nonlinearity, here applied in the RFID case, could be certainly extended toward many other contexts also requiring dc energy sources.

References

[1] L. Yan, Y. Zhang, L. Yang, H. Ning, The Internet of Things: from RFID to the Next-Generation Pervasive Networked Systems, Wireless Networks and Mobile Communications, CRC Press, Boca Raton, FL, USA, 2008.
[2] G. Marrocco, Pervasive electromagnetics: sensing paradigms by passive RFID technology, IEEE Trans. Wirel. Commun. 17 (6) (2010) 10–17.
[3] H. Solar, A. Beriain, I. Zalbide, E. D'Entremont, R. Berenguer, A robust −40° to +150 °C wireless rotor temperature monitoring system based on a fully passive UHF RFID sensor tag, in: Proc. IEEE International Microwave Symposium, Tampa Bay, FL, USA, 1–6 June 2014.
[4] S. Rima, A. Georgiadis, A. Collado, R. Goncalves, N. Carvalho, Passive UHF RFID enabled temperature sensor on cork substrate, in: Proc. IEEE International Conference on RFID Technology and Applications, Tampere, Finland, 8–9 September 2014.
[5] A. Faul, J. Naber, Design and test of a 915 MHz RFID-based pressure sensor for glaucoma, in: Proc. IEEE Latin America Symposium on Circuits and Systems, Santiago, Chile, 25–28 February 2014.
[6] J. Gao, J. Siden, H-E. Nilsson, M. Gulliksson, Printed humidity sensor with functionality for passive RFID tags, IEEE Sens. J. 13 (5) (2013) 1824–1834.
[7] R.S. Nair, E. Perret, S. Tedjini, T. Baron, A group-delay-based chipless RFID humidity tag sensor using silicon nanowires, IEEE Antennas Wirel. Propag. Lett. 12 (2013) 729–732.
[8] S. Caizzone, E. DiGiampaolo, Passive RFID deformation sensor for concrete structures, in: Proc. IEEE International Conference on RFID Technology and Applications, Tampere, Finland, 8–9 September 2014.
[9] S. Caizzone, E. DiGiampaolo, G. Marrocco, Wireless crack monitoring by stationary phase measurements from coupled RFID tags, IEEE Trans. Antennas Propag. 62 (12) (2014) 6412–6419.
[10] J. Grosinger, J. Griffin, Backscatter RFID sensor with a bend transducer, US Patent US 2014/0049421A1, 2014.
[11] M. Cremer, U. Dettmar, R. Kronberger, C. Hudasch, V. Wienstroer, Passive UHF RFID transponders for switching and controlling, in: Proc. IEEE International Conference on RFID Technologies and Applications, Johor Bahru, Malaysia, 4–5 September 2013.
[12] S. Manzari, A. Catini, G. Pomarico, C. Di Natale, G. Marrocco, Development of an UHF RFID chemical sensor array for battery-less ambient sensing, IEEE Sens. J. 14 (10) (2014) 3616–3623.
[13] S.D. Nguyen, T.T. Pham, E.F. Blanc, N.N. Le, C.M. Dang, S. Tedjini, Approach for quality detection of food by RFID-based wireless sensor tag, Electron. Lett. 49 (25) (2013) 1588–1589.
[14] E.M. Amin, J.K. Saha, N.C. Karmakar, Smart sensing materials for low-cost chipless RFID sensor, IEEE Sens. J. 14 (7) (2014) 2198–2207.
[15] R. Bhattacharyya, C. Floerkemeier, S. Sarma, Low-cost, ubiquitous RFID-tag-antenna-based sensing, Proc. IEEE 98 (9) (2010) 1593–1600.
[16] C. Occhiuzzi, G. Marrocco, Constrained-design of passive RFID sensor antennas, IEEE Trans. Antennas Propag. 61 (6) (2013) 2972–2980.
[17] L. Catarinucci, R. Colella, L. Tarricone, Enhanced UHF RFID sensor-tag, IEEE Microw. Wirel. Compon. Lett. 23 (1) (2013) 49–51.
[18] J. Grosinger, W. Bosch, A passive RFID sensor tag antenna transducer, in: Proc. European Conference on Antennas and Propagation, The Hagues, The Netherlands, 6–11 April 2014, pp. 3638–3639.
[19] D. De Donno, L. Catarinucci, L. Tarricone, A battery-assisted sensor-enhanced RFID tag enabling heterogeneous wireless sensor networks, IEEE Sens. J. 14 (4) (2014) 1048–1055.

[20] Y. Su, A. Wickramasinghe, D.C. Ranasinghe, Investigating sensor data retrieval schemes for multi-sensor passive RFID tags, in: Proc. IEEE International Conference on RFID, San Diego, CA, USA, 15–17 April 2015, pp. 158–165.
[21] A.E. Abdulhadi, R. Abahri, Multiport UHF RFID tag antenna for enhanced energy harvesting of self-powered wireless sensors, IEEE Trans. Ind. Inform. 12 (2) (2016) 801–808.
[22] Y. Duroc, G. Andia Vera, Towards autonomous wireless sensors: RFID and energy harvesting solutions, in: S.C. Mukhopadhyay (Ed.), Internet of Things, Challenges and Opportunities, Springer-Verlag, 2014.
[23] M.M. Islam, K. Rasilainen, V. Viikari, Implementation of sensor RFID: carrying sensor information in the modulation frequency, IEEE Trans. Microw. Theory Tech. 63 (8) (2015) 2672–2681.
[24] V. Talla, J.R. Smith, Hybrid analog-digital backscatter: a new approach for battery-free sensing, in: Proc. IEEE International Conference on RFID, Orlando, FL, USA, 30 April–2 May 2013.
[25] A.P. Sample, D.J. Yeager, P.S. Powledge, A.V. Mamishev, J.R. Smith, Design of an RFID-based battery-free programmable sensing platform, IEEE Trans. Instrum. Meas. 57 (11) (2008) 2608–2615.
[26] G. Andia Vera, Y. Duroc, S. Tedjini, RFID test platform: non-linear characterization, IEEE Trans. Instrum. Meas. 63 (9) (2014) 2299–3005.
[27] G. Andia Vera, Y. Duroc, S. Tedjini, Analysis of harmonics in UHF RFID signal, IEEE Trans. Microw. Theory Tech. 61 (6) (2013) 2481–2490.
[28] J.G. Vogler, D.J. Maquire, A.E. Steinhauer, DINADE – a new interrogation, navigation and detection system, Microw. J. 10 (4) (1967) 2–6.
[29] J. Song, V. Viikari, N. Pesonen, I. Marttila, H. Seppa, Optimization of wireless sensors based on intermodulation communication, IEEE Trans. Microw. Theory Tech. 61 (9) (2013) 3446–3452.
[30] K. Rasilainen, J. Ilvonen, A. Lehtovuori, J-M. Hannula, V. Viikari, On design and evaluation of harmonic transponders, IEEE Trans. Antennas Propag. 63 (1) (2015) 15–23.
[31] J-M. Hannula, K. Rasilainen, V. Viikari, Characterization of transponder antennas using intermodulation response, IEEE Trans. Antennas Propag. 63 (6) (2015) 2412–2420.
[32] H. Kwun, G.L. Burkhardt, J.L. Fisher, Detection of reinforcing steel corrosion in concrete structures using non-linear harmonic and intermodulation wave generation, U.S. Patent 5 180 969, 19 January 1993.
[33] M. Ritamaki, A. Ruhanen, V. Kukko, J. Miettinen, L.H. Turner, Contactless radiation pattern measurement method for UHF RFID transponders, Electron. Lett. 41 (13) (2005) 723–724.
[34] C. Mariotti, G. Orecchini, F. Alimenti, P. Cosseddu, P. Mezzanotte, A. Bonfiglio, L. Roselli, M. Virili, G. Casula, 7.5–15 MHz organic frequency doubler made with pentacene-based diode and paper substrate, in: Proc. IEEE International Microwave Symposium, Tampa Bay, FL, USA, 1–6 June 2014.
[35] V. Palazzi, P. Mezzanotte, L. Roselli, Design of a novel antenna system intended for harmonic RFID tags in paper substrate, in: Proc. IEEE Conference on Wireless Power Transfer, Boulder, CO, USA, 13–15 May 2015.
[36] H. Gomes, N.B. Carvalho, RFID for location proposes based on the intermodulation distortion, Sens. Transducers J. 106 (7) (2009) 85–96.
[37] P.V. Nikitin, K.V.S. Rao, Harmonic scattering from passive UHF RFID tags, in: Proc. IEEE Antennas and Propagation International Symposium, Charleston, SC, USA, 1–5 June 2009.
[38] G. Andia Vera, Y. Duroc, S. Tedjini, Third harmonic exploitation in passive UHF RFID, IEEE Trans. Microw. Theory Tech. 63 (9) (2015) 2991–3004.
[39] S. Tedjini, Y. Duroc, G. Andia Vera, C. Loussert, M. Recouly, RFID communication system, US Patent 2015/0288424 A1, 8 October 2015.
[40] G. Andia Vera, D. Allane, A. Georgiadis, A. Collado, Y. Duroc, S. Tedjini, Cooperative integration of harvesting RF sections for passive RFID communication, IEEE Trans. Microw. Theory Tech. 63 (12) (2015) 4556–4566.
[41] J.A. Hagerty, F.B. Helmbrecht, W.H. McCalpin, R. Zane, Z.B. Popovic, Recycling ambient microwave energy with broad-band rectenna arrays, IEEE Trans. Microw. Theory Tech. 52 (3) (2004) 1014–1024.
[42] M.S. Trotter, J.D. Griffin, G.D. Durgin, Power-optimized waveforms for improving the range and reliability of RFID systems, in: Proc. IEEE International Conference on RFID, 27–28 April 2009, pp. 80–87.
[43] D. Allane, G. Andia Vera, Y. Duroc, R. Touhami, S. Tedjini, Harmonic power harvesting system for passive RFID sensor tags, IEEE Trans. Microw. Theory Tech. 64 (7) (2016) 2347–2356.
[44] EM Microelectronic-Marin SA, [Online]. Available: http://www.emmicroelectronic.com/sites/default/files/public/products/datasheets/4325-ds.pdf.